

PCCP

Accepted Manuscript



This is an *Accepted Manuscript*, which has been through the Royal Society of Chemistry peer review process and has been accepted for publication.

Accepted Manuscripts are published online shortly after acceptance, before technical editing, formatting and proof reading. Using this free service, authors can make their results available to the community, in citable form, before we publish the edited article. We will replace this *Accepted Manuscript* with the edited and formatted *Advance Article* as soon as it is available.

You can find more information about *Accepted Manuscripts* in the [Information for Authors](#).

Please note that technical editing may introduce minor changes to the text and/or graphics, which may alter content. The journal's standard [Terms & Conditions](#) and the [Ethical guidelines](#) still apply. In no event shall the Royal Society of Chemistry be held responsible for any errors or omissions in this *Accepted Manuscript* or any consequences arising from the use of any information it contains.

***ab initio* Kinetic Monte Carlo simulations of dissolution at the NaCl-water interface**Jian-Cheng Chen^{1,2}, Bernhard Reischl^{1,3}, Peter Spijker¹, Nico Holmberg², Kari Laasonen^{1,2}, and Adam S. Foster¹¹*COMP Centre of Excellence and Department of Applied Physics, Aalto University, FI-00076, Helsinki, Finland*²*Department of Chemistry, Aalto University, FI-00076 Helsinki, Finland and*³*Department of Physics, University of Helsinki, FI-00014 Helsinki, Finland*

(Dated: August 28, 2014)

We have used *ab initio* molecular dynamics (AIMD) simulations to study the interaction of water with the NaCl surface. As expected, we find that water forms several ordered hydration layers, with the first hydration layer having water molecules aligned so that oxygen atoms are on average situated above Na sites. In an attempt to understand the dissolution of NaCl in water, we have then combined AIMD with constrained barrier searches, to calculate the dissolution energetics of Na⁺ and Cl⁻ ions from terraces, steps, corners and kinks of the (100) surface. We find that the barrier heights show a systematic reduction from the most stable flat terrace sites, through steps to the smallest barriers for corner and kink sites. Generally, the barriers for removal of Na⁺ ions are slightly lower than for Cl⁻ ions. Finally, we use our calculated barriers in a Kinetic Monte Carlo as a first order model of the dissolution process.

1. INTRODUCTION

The dissolution of sodium chloride (NaCl) into liquid water is a very common phenomenon in our everyday life, and can readily be verified by dropping a spoonful of table salt in a glass of water. However, the dissolution process is not well understood on the molecular level, and yet it remains key in a variety of processes, such as atmospheric chemistry and in particular cloud electrification and coastal erosion [1]. As is the general case for studying crystal growth and dissolution [2–6], the specific atomic structure at the interface between the crystal and water, and especially the hydration structure, plays a crucial role in the dissolution mechanism.

An obvious approach to investigate the dissolution process in atomic detail is via simulation. However, theoretical modeling of these processes is hindered by the gap between the time and length scales of the macroscopic dissolution and those of the underlying atomic processes. A single ionic dissolution is a rare event, which is unlikely to happen on the time scale of a molecular simulation, and therefore the dissolution needs to be driven artificially. But since this is a complex mechanism, involving collective solvent dynamics, the choice of an appropriate ‘reaction coordinate’ is generally non-trivial, and care must be taken to ensure sufficient sampling of all the degrees of freedom orthogonal to the reaction coordinate(s). The system sizes and time necessary to model the dissociation still pose a huge challenge to an approach based on *ab initio* molecular dynamics. While it is possible to study the adsorption energetics and geometries of individual water molecules, or even full molecular layers, on crystal surfaces from first principles [7–11], studies dealing with fully solvated systems of NaCl surfaces, or ion pairs, usually resort to empirical interaction potentials [12–15]. As this significantly reduces the computational effort, it is possible to obtain sufficient statistics to take entropic contributions from the solvent into account. However, different empirical potentials may demonstrate significant variability in energetics of water molecules in hydration layers and ions in the crystal surface [16].

Recently, *ab initio* molecular dynamics simulations have been used to study the initial stages of the NaCl dissociation in water [17–20]. Using metadynamics and transition path sampling, these simulations identified the dissolution reaction pathway for Na⁺ and Cl⁻ ions from a kink, and calculated the dissolution free energy profile. Our own recent study [21], explored the

dissolution of small NaCl clusters and determined that the difference between dissolution of Na⁺ and Cl⁻ arises due to faster water mediated elongations of individual ionic bonds to Na⁺, but a significantly slower process for the last bond in comparison to Cl⁻. In the present study, we calculate free energy barriers of dissolution for different surface sites (e.g., edges, corners, kinks, etc.), using *ab initio* molecular dynamics simulations (AIMD). This study complements and extends these previous AIMD studies, as we focus on all possible dissolution sites and determine their free energy barriers. To the best of our knowledge this rigorous approach is the first of its kind at this scale. Based on these free energy barriers and appropriate attempt frequencies, we are able to determine reaction rates for the dissolution from each of the possible surface sites, which can then be used to construct a Kinetic Monte Carlo (KMC) model. This allows us to bridge the time scales between the atomistic details and the microscopic dissolution mechanism of an extended system of NaCl in water, shedding light on the entire pathway of the dissolution of a larger NaCl crystal.

The remainder of this article is organized as follows: in Section 2, we present simulations of the NaCl/water interface based on empirical atomistic interaction potentials using classical molecular dynamics, serving as a preparation platform and statistical benchmark for the AIMD simulations which are subsequently presented in Section 3. These simulations are performed to systematically compute dissolution barriers for Na⁺ and Cl⁻ ions from the different surface sites. In Section 4, we present the KMC simulations of the dissolution of an extended NaCl surface and nanocluster. Finally, in Section 5, we summarize our results and give a critical assessment of the strengths and limitations of the methodology employed in this study.

2. CLASSICAL MOLECULAR DYNAMICS STUDY

In order to assess the minimum system size necessary to describe the hydration layer structures at the NaCl(100)/water interface correctly, we performed molecular dynamics (MD) simulations with an empirical interaction potential based on the OPLS-AA description of Na⁺ and Cl⁻ ions, and the SPC/E model of water [22], using the GROMACS simulation package [23]. The reference system consisted of a $p(4 \times 4)$ slab of NaCl(100), 6 layers thick, and ~ 1000 water molecules in periodic boundary conditions. The thickness of the water volume between periodic images of the NaCl slab was sufficient that hydration structures on either side of the slab would not interact. This system is simulated for 10 ns at a temperature of 300 K and pressure of 1 bar, using a Nosé-Hoover thermostat [24, 25] and a Parrinello-Rahman barostat [26]. Several smaller systems, with a water layer of finite thickness on top of the NaCl slab are created as well, and are run for 10 ns in NVT to collect good statistics on hydration layer structures, and assess the errors introduced by finite size effects as well as the presence of a second interface to vacuum. The water molecules' oxygen atom density profiles along the direction perpendicular to the surface, shown in Figure 1, indicate the presence of at least two well defined hydration layers at the NaCl(100)/water interface, which are located around 2.4 and 6.2 Å and are in good agreement with previous MD simulations [27, 28]. For all the small systems studied, the introduction of a second interface to the vacuum did not affect the position and height of the first and second peaks in the oxygen density, compared to the reference system. A small peak in oxygen density at the water/vacuum interface is introduced, but the lateral water distributions within the first two hydration layers remained unaffected. We chose the $p(4 \times 4)$ cell with 256 water molecules, and the $p(3 \times 3)$ cell with 144 water molecules for further studies using *ab initio* molecular dynamics, and used the equilibrated output of the classical simulation as starting configurations. This size of system is also compatible with the ordering scale predicted in earlier experimental studies [29].

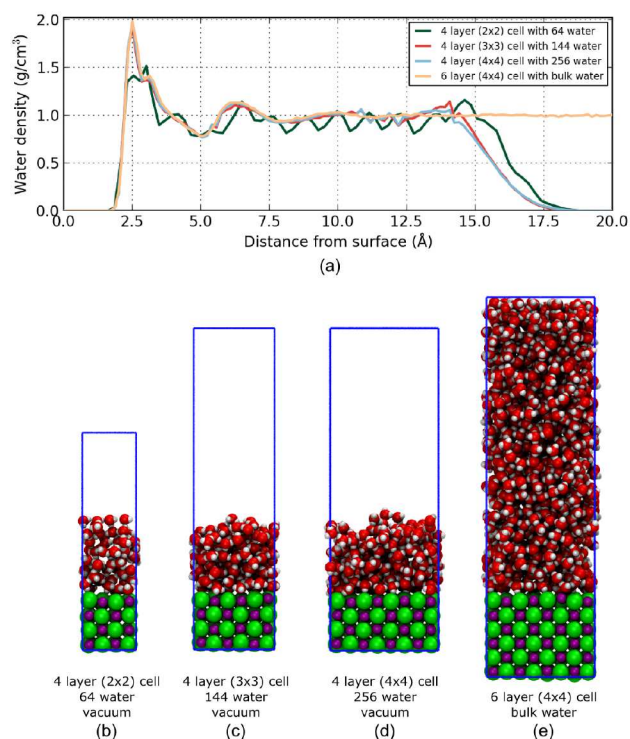


FIG. 1: (a) Water molecule density profiles (smoothed using a Gaussian filter) as a function of the distance to the NaCl(100) surface, obtained from classical MD simulations for the following system sizes: (b) four layer $p(2 \times 2)$ NaCl cell with 64 water molecules, (c) four layer $p(3 \times 3)$ cell with 144 water molecules, (d) four layer $p(4 \times 4)$ cell with 256 water molecules, and (e) six layer $p(4 \times 4)$ cell and bulk water. The purple and green spheres represent Na^+ and Cl^- ions, and the red and white spheres represent O and H atoms of water molecules, respectively.

3. *AB INITIO* MOLECULAR DYNAMICS SIMULATIONS

To perform the *ab initio* molecular dynamics simulations (AIMD) we used the CP2K code with the QUICKSTEP module [30], where the basis set is a hybrid of Gaussians and plane waves. The Perdew-Burke-Ernzerhof (PBE) functional [31, 32] is employed to describe the exchange and correlation energies. Van der Waals interactions are calculated using DFT-D3, in which both the pairwise dispersion correction term C_6R^{-6} and three body correction term C_9R^{-9} are included [33]. A plane wave cutoff energy of 270 Ry. was found to converge the full system's equilibrium structure well in comparison to experimental data - very minor differences were seen in the structure of water at higher cutoffs. For sodium, the different pseudopotentials and plane wave cutoff were tested in our earlier work [21]. In this work used a one-electron pseudopotential for Na - this is well converged within 270 Ry cutoff and gives comparable results to a larger 9-electron pseudopotential with 600 Ry cutoff. Hydrogen atoms were replaced by Deuterium, to enable a larger time step of 1 fs. The temperature was kept constant at 348.15 K using a Nosé-Hoover chain thermostat [24, 25] with a time constant of 300 fs, to obtain the correct diffusion coefficient of water as if it is at room temperature.

Starting from system configurations obtained with the classical potentials described above, we calculated 54 ps AIMD trajectories of a $p(4 \times 4)$ NaCl slab with 256 water molecules, and a smaller $p(3 \times 3)$ NaCl slab with 144 water molecules. Periodic boundary conditions are applied in x , y , and z . In the z -direction periodic images of the NaCl slab are separated by 20 Å to

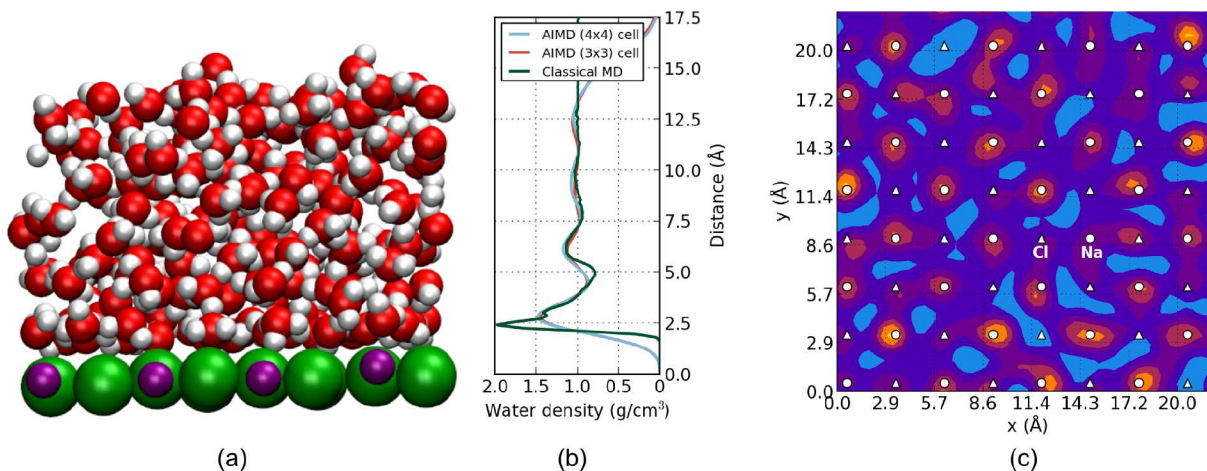


FIG. 2: In (a) a representative snapshot of the water structure from the AIMD simulations is shown. The same color scheme to color the atoms is used as in Fig 1. In (b) the water density distribution perpendicular to the NaCl(100) surface is shown both for the (3x3) and (4x4) system. This density profile is aligned with the snapshot in (a). In (c) the lateral density profile for the first hydration layer on top of the NaCl(100) surface is shown (blue indicating low density and yellow a high density). Here, the white circles indicate a spot in the underlying crystals being occupied by a Na^+ ion and similarly the white triangles indicate a Cl^- ion.

avoid spurious interactions, introducing a vacuum above the water molecules. The AIMD trajectory is significantly longer than the time scale of hydrogen bond network fluctuations (approximately 0.5 ps [34, 35]), and therefore we assume that the results are essentially not correlated to the starting configuration obtained from classical dynamics.

A. Hydration layer structure

In Figure 2 a representative snapshot of our simulations is shown together with the hydration layer structures on the $p(4 \times 4)$ and $p(3 \times 3)$ NaCl slabs (as measured by looking at the water oxygen density perpendicular to the surface) compared to the results from the classical MD simulations. The water density profiles perpendicular to the surface have been smoothed using a Gaussian filter of width 0.2 Å. The density profiles perpendicular to the surface obtained from first principles are very similar to the ones obtained with empirical potentials: the first peak in water density corresponding to the position of the first hydration layer is around 2.5 Å above the surface, and a second peak can be clearly observed at 6.2 Å. The fourth peak around 13 Å is caused by the second interface between liquid layer and vacuum, and the third peak around 9 Å might be caused by the presence of both interfaces simultaneously. The height of the first peak in the AIMD simulation, after applying the Gaussian filter, is 1.44 g/cm³, which is in good agreement with the density maximum of 1.40 g/cm³, observed previously by Liu *et al.* [17–19] on top of a smaller $(3\sqrt{2} \times 4\sqrt{2})R45^\circ$ cell.

The lateral density plot within the first hydration layer (Figure 2c) confirms that water molecules in the first hydration layer are situated mostly over Na^+ ions. This agrees with theoretical work by Yang *et al.* [36], however as our system is larger, we can exclude artificial over-structuring due to lateral periodicity. Some water molecules also reside over Cl^- ions, which corresponds to the shoulder in the first peak of the density profile along z . Water molecules further away from the surface than this first layer do not exhibit any strong lateral ordering in our simulations.

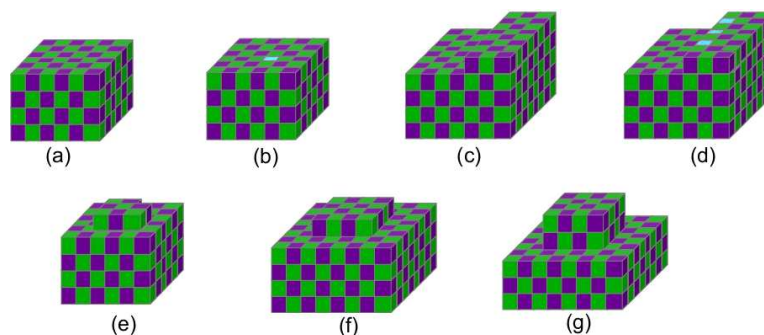


FIG. 3: Models of the different NaCl(100) surfaces used in the computation of the energy barriers. The purple and green cubes represent Na^+ and Cl^- ions, respectively, whereas the light blue cubes represent vacancy sites. The numbering of the models corresponds to the numbering used in the text.

B. Dissolution energy barriers

So far we have only considered flat NaCl surfaces of different sizes and only focused on the water structuring on these surfaces from a classical and *ab initio* point of view. In the case of ion dissolution, if we consider a perfect, infinite surface, it is clear the first step is the dissolution of either a Na^+ or Cl^- ion, creating a vacancy in the otherwise flat surface. Following this, it is very plausible that the energy barrier for the dissolution of an ion adjacent to the vacancy is different from the barrier in the case of the dissolution from the flat surface. As the dissolution process continues, different types of surface sites will appear each with its own dissolution energy barrier. Of course, for a real NaCl crystal surface, many of these sites will exist even before the dissolution process begins. For the NaCl(100) surface we have identified the following seven possible surface sites (see also Figure 3) for either a Na^+ or a Cl^- ion: a) an ion within the flat surface, b) an ion adjacent to a vacancy within the flat surface, c) an ion on a step edge, d) an ion on a step edge adjacent to a vacancy, e) an ion at a kink site (one layer island), f) an ion at another kink site (one layer island), and g) an ion at corner site (two layer island). We would like to point out that in the previous studies of the NaCl-water interface [17–19] only configuration e) was considered, although later studies of water adsorption considered further sites [20]. For each of those systems we have performed AIMD simulations and for comparison reasons we have also conducted some of the simulations with both the $p(3 \times 3)$ and the $p(4 \times 4)$ cell.

To calculate the different energy barriers for the dissolution of Na^+ and Cl^- ions for each of these seven surface sites (14 different systems when considering both the Na^+ and the Cl^- ions) we used the constraint method [37]. In this method the radial distance between an ion initially within the surface and the center of mass of the 12 closest ions in one of the layers underneath it is constrained to a certain value r . By integrating the average force $\langle F(r) \rangle$ acting along the direction of the constraint distance vector \mathbf{r} , the free energy profile as a function of the constraint distance r can be calculated [38] as

$$E(r) = \int_{r_1}^{r_2} \langle F(r) \rangle dr, \quad (1)$$

where r_1 and r_2 denote the initial and final constraint distances, respectively. The forces we obtain are averaged over 10 ps at each value of the constraint distance, and then interpolated using a cubic spline. The barriers are converged to within a standard error of 0.05 eV. Note that at the barrier position, the constraint force $\langle F(r_b) \rangle_T$ should be zero in principle. From the free energy surface map in Ref. [19], we conclude that the distance between the ion and the surface by itself is a satisfactory reaction coordinate, so we have converted our constraint distance into the same reaction coordinate as well, and in the remainder we always refer

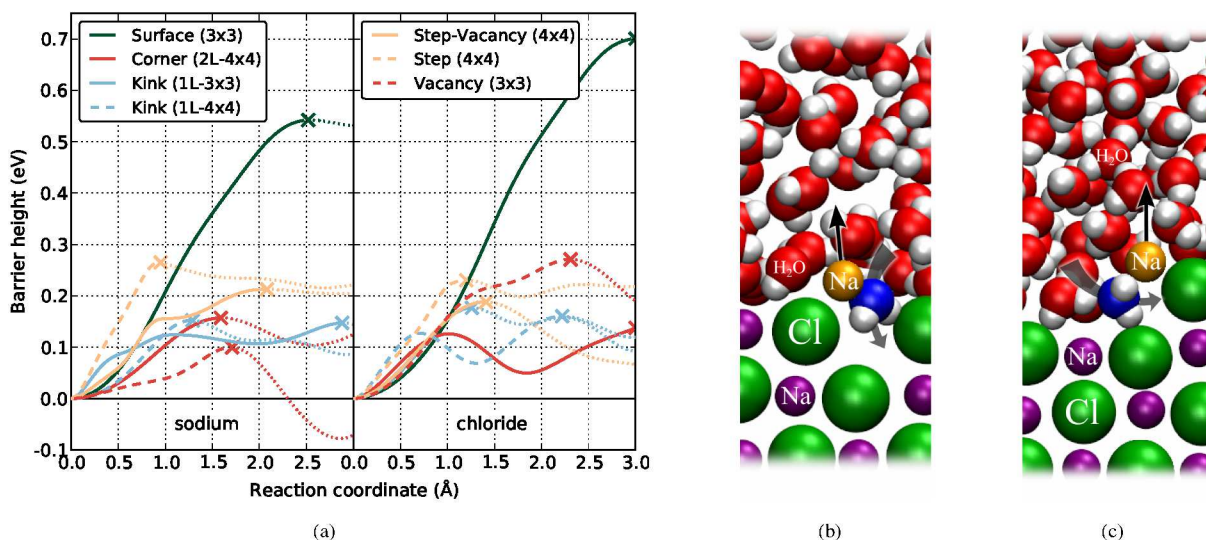


FIG. 4: In (a) for either Na^+ (left) or Cl^- (right) ions the dissolving barriers as a function of the reaction coordinate are shown for all seven possible positions as explained in the text (different colors and line style, see legend). The crosses mark the maximum value for the respective barrier. In the legend the system, either $p(3 \times 3)$ or $p(4 \times 4)$, or one (1L) or two (2L) layer islands is indicated in the brackets. In (b) and (c) the process of the dissolution of an ion using the constraint method is shown in side view for both a flat surface (b) and a step edge (c). In both cases a water molecule (in blue) can be seen to occupy the space left behind by the dissolving ion (in orange). More details of the dissolution process can be seen in the movies in the Supplementary Information.

to this converted reaction coordinate. The energy barrier for dissolving was taken as the first maximum encountered in the free energy profile before reaching to cutoff at 3.0 \AA . When using this constrained method the configurational space available to the constrained ion is reduced, and as such the free energy should be corrected for by adding a purely entropic contribution of $2 k_B T \ln r$ (see supplementary information of ref. [39]). However, in the present study this correction term is smaller than the error in the free energy calculation, and can therefore be safely ignored. Comparisons to metadynamics approaches [19, 21], including committer tests around the transition state [19], indicate that this reaction coordinate is a reasonable choice.

In Figure 4(a) the free energy profiles we computed are shown for all systems, with the Na^+ ions on the left and the Cl^- ions on the right. In this figure the colors indicate the different surface sites (see above and legend) and the value we considered to be the barrier height is indicated by a cross mark. We would like to point out that we have computed the free energy profile for each of the systems up to at least 3.0 \AA , but in the figure we deliberately dotted the lines after reaching the barriers as typically the results of the constrained method are less accurate after this barrier as much greater sampling is needed in less ordered water layers. In Table I we also list the values for each of the barriers, indicating also whether the simulations are for the $p(3 \times 3)$ or $p(4 \times 4)$ cell systems.

From our results it is clearly visible that regardless of the type of ion, the dissolution of an ion from the flat surface has the highest barrier (0.54 eV for Na^+ and 0.70 eV for Cl^-). Once a surface atom is removed the barrier of dissolution drops considerably and after a few more atoms are dissolved the barriers reach a lowest value of 0.14 eV for a kink site on a one layer island. This agrees with the earlier atomic force microscope (AFM) experimental works by Dai *et al.* [40], that the water molecule adsorptions were observed at the step edges when the NaCl surface is exposed at low RH (less than 35 %). They also found that the steps on the NaCl(100) surface flow very easily and become invisible at a high RH of 73 % [40]. This should

TABLE I: Barrier heights (eV) and vibrational frequencies (cm^{-1}) for different sites at the NaCl(100) surface when dissolving an ion into water.

Surface site	Barrier for Na^+	Barrier for Cl^-	Vibr. freq. for Na^+	Vibr. freq. for Cl^-
Flat $p(3 \times 3)$	0.54	0.70	146	141
Vacancy $p(3 \times 3)$	0.10	0.27	169	150
Step $p(4 \times 4)$	0.26	0.23	174	158
Step vacancy $p(4 \times 4)$	0.23	0.18	174	158
Kink (one layer island) $p(3 \times 3)$	0.14	0.17	166	140
Kink (one layer island) $p(4 \times 4)$	0.15	0.12	166	140
Corner (two layer island) $p(4 \times 4)$	0.15	0.12	166	140

correspond to the dissolving process of the step and related kink sites.

In the case of the dissolution from the flat surface a clear barrier seems to be absent (e.g., the free energy for Cl^- reaches its maximum at the highest value for the reaction coordinate, green line in right figure), as either it keeps increasing or plateaus. However, if we release the constraint in the simulation at the distance where we assume the barrier height is at its maximum, the ions do not return to their vacated surface sites within 14 ps. In fact, after the ion has moved far enough away from the surface, a water atom will take its place in the surface and, thus, fills the vacancy. In fact, in each of the cases the dissolving ion leaves a vacancy behind it will always be filled with a water molecule, see Figures 4(b-c) ¹.

To put these dissolution barriers from a completely flat surface into perspective we have also performed one simulation where we dissolve a Cl^- ion from a flat surface but without the water. In this case the energy barrier for dissolution is at 3.67 eV, significantly higher than in the fully hydrated case, indicating the importance of water in catalyzing the dissolution process of the neighboring ion.

The relatively high barriers for the detachment of Na^+ and Cl^- ions indicate that the flat surface of NaCl(100) surface is inert, which agrees with the AIMD results discussed previously that the water contacted $p(4 \times 4)$ and $p(3 \times 3)$ surfaces are stable after 54 ps of propagation. This result also agrees with the previous AIMD result by Liu *et al.* [17, 18], but disagrees with the previous DFT works by Cabrera-Sanfeliix *et al.* [41] that dissolving Cl^- ion from the NaCl(100) surface experiences a very low barrier about 0.05 eV at high relative humidity (RH). The location of their barrier position is also closer to the surface at about $Z = 2.0 \text{ \AA}$, which is probably due to the surface temperature being set to 0 K. For the kink site atoms, the dissolving barriers are both around 0.15 eV. The Cl^- ion dissolving barrier height agrees very well with the previous result of 0.13 eV [19]. However, in their work, the Na^+ ion dissolving from the kink site experiences a much larger dissolving barrier of 0.3 eV, which should indicate that the Cl^- ions will dissolve into liquid water at first.

4. KINETIC MONTE CARLO

To bridge the gap between the time scale of the atomistic processes leading to the dissolution of a single Na^+ or Cl^- ion from a given surface site, and the time scale of the dissolution of a microscopic NaCl crystal, we use a Kinetic Monte Carlo

¹In the supplementary information available online there is a movie showing in detail the dissolution process and vacancy occupation mechanism as depicted in Figures 4(b-c).

(KMC) approach [42, 43], which allows us to accurately describe this dissolution process based on our AIMD kinetics. In a KMC simulation several events (dissolution from a flat surface, kink site, etc.) happen based on a rate R_{ij} computed from transition state theory, which depends on the nature of the site i , the type of ion j and the temperature T . Furthermore, the time between two (different or similar) events in the KMC simulation depends also on the same rate $R_{ij} = v_{ij}e^{-E_{ij}/k_B T}$, where E_{ij} is the free energy barrier previously computed for the specific site (i) and ion (j), v_{ij} its vibrational frequency obtained from the Fourier transform of the respective atomic trajectory in the AIMD barrier search, and k_B is the Boltzmann constant. All vibrational frequencies we computed can also be found in Table I. In our KMC simulations, only the forward dissolving process is considered - the backward process of NaCl surface growth is ignored for simplicity. Furthermore, kink sites and step vacancy sites are all approximated as corner sites since the barriers are the same within our AIMD errors.

Using this KMC method, the dissolution of a periodic NaCl(100) surface and a finite cubic NaCl crystal are investigated. For the periodic surface, we used a $(50 \times 50 \times 5)$ supercell, with a surface area of 812 nm^2 and containing 10 000 Na and Cl atoms in each layer. Periodic boundary conditions are applied along x and y directions, parallel to the surface, and the bottom layer is fixed to resemble the bulk structure. The NaCl nanocrystal is modeled by a $(25 \times 25 \times 25)$ supercell, with 14 nm side length and containing 125 000 atoms.

On the defect-free, periodic NaCl(100) surface the first ion dissolution occurs at 1382 ns. After this event a vacancy has appeared in the surface, and as a consequence the time step in the KMC algorithm rapidly decreases and only after an additional 4 ns the time step has reached its smallest value of 365 fs (about 4 order of magnitudes faster). This decrease is a direct consequence of the occurrence of step, kink and corner sites while more and more ions are dissolved. When the time step has reached its minimal value approximately half of the surface atoms in the first layer (5000 atoms) have dissolved. For the next 2 ns the time step remains this small, but then rapidly increases as there are less and less step, kink and corner sites available, eventually leading to the complete dissolution of the first layer. After the first layer has completely dissolved, the second layer starts dissolving in a similar way, including a comparable waiting time before the first dissolution event occurs. In Figure 5(a) four representative snapshots of the dissolution of the first layer are shown, illustrating how the process starts from an initial atomic defect. From this figure it can also be inferred that during the process of dissolution the number of ions of either site type changes dynamically, which is shown in Figure 5(b). Over the entire process the number of step sites increases faster than any other site type (except the surface site type) and has a maximum of 280 just before the dissolution starts to slow down. In comparison the maximum number of kink sites is 70, whereas the number of vacancies at the steps never comes above 15. It is worth noting that the number of surface sites never falls below the number of any of the other site types.

The dissolution of the NaCl nanocrystal differs considerably from the periodic slab, as already from the start possible nucleation sites for dissolution exist (corners and steps along the edges of the cube). The first event already occurs at 761 fs and the time step rapidly decreases to 40 fs when about 5000 atoms are dissolved (compared to 365 fs after the same amount of dissolved ions in the case of the periodic slab). As corner sites are more likely dissolved than step sites, the initially cubic nanocrystal gradually becomes more spherical as can be seen in Figure 6(a). A very recent AFM study by Bruzewicz *et al.* [44], has shown that a 83 nm NaCl nano particle's corner rounding up at a relative humidity of 52 %, which agrees with our KMC predictions as shown in Figure 6(a) (c – d) where the corners of the 14 nm crystal disappear. Because in our KMC approach crystal regrowth is excluded, the nanocrystal becomes as spherical as it can be and as a consequence the number of corner (or kink) and step atoms keeps increasing with time, see Figure 6(b). After approximately 1.2 ns the number of step sites exceeds the number of surface sites and, similarly, after 1.4 ns the number of surface sites falls below the number of corner sites as well. Also, both the number of corner and step sites keeps increasing and only start to level off because of the finite size of the nanocrystal. On

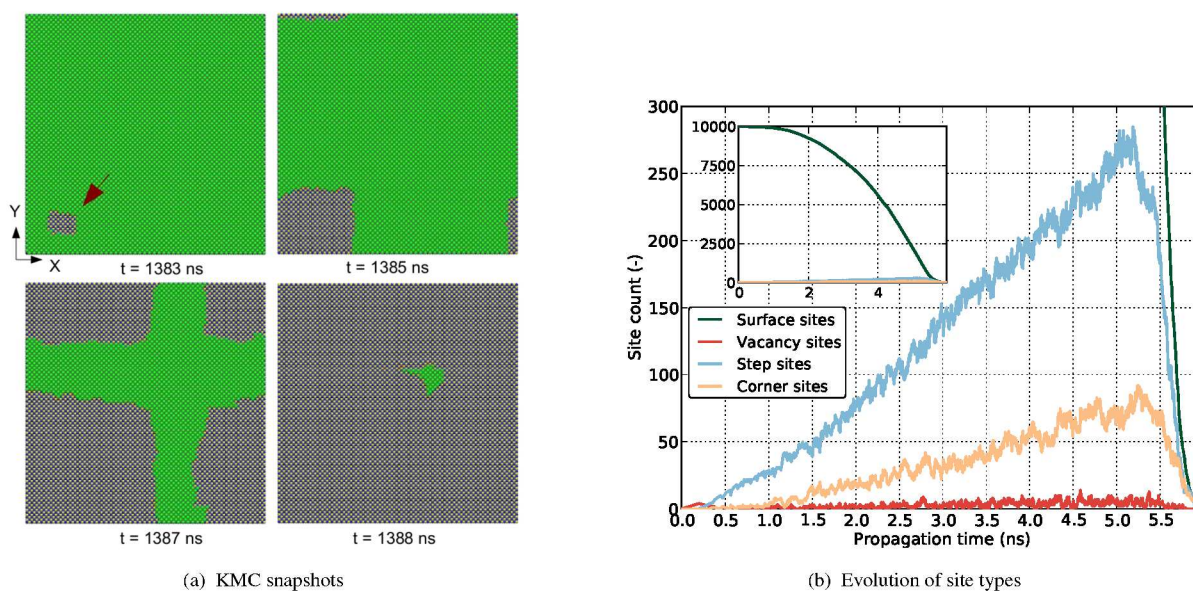


FIG. 5: In (a) four snapshots at different times in the KMC dissolution for the periodic slab simulation are shown. Atoms in the first layer are in green and gray for the second layer. The arrow in the top left figure shows the site where the dissolution nucleates. In (b) the evolution of the number of surface, vacancy, step and corner (kink) sites during the dissolution is depicted. The inset in (b) shows the entire range of surface site numbers. Time is measured since the first dissolution event at 1382 ns and during the displayed time only the atoms in the first layer dissolve.

the other hand, the number of vacancy sites remains more or less constant at around 450. Even for smaller nanocrystals ($11 \times 11 \times 11$ supercell) with or without initial defects like steps or vacancies the same dissolution process (from cube to spherical) is observed, although the initial time step size may be different.

In both cases the majority of ions dissolve via corner/kink site (88% and 92% for the periodic and nanocrystal system, respectively) or via step sites (11% vs. 7%), and both the vacancy or surface sites make up about 1% for both systems. Similarly, when looking at the total probabilities for each site to dissolve (i.e., the sum of each individual probability at each time step for the given site type) it is clear that corners are favored (87%) over the steps (10%), vacancies (3%) or surface sites (less than 1%). Only in the initial onset of dissolution these probabilities are different, especially for the periodic slab as it needs at least one surface site atom to dissolve, before any other mechanism can kick in.

5. DISCUSSION

In this work we have studied the dissolution process of a NaCl crystal using both a first principles and kinetic approach. We have first shown that our *ab initio* MD method is in good agreement with results obtained from classical MD simulations. Subsequently we have systematically determined the energy barriers an Na^+ or Cl^- ion encounters when dissolving from all possibly different sites (surface, kink, step, etc.) of the crystal. Based on characteristics obtained from these AIMD simulations we constructed a Kinetic Monte Carlo model that we used to study much larger NaCl systems, which are unfeasible to model with either *ab initio* or classical MD simulations. We have shown that most of the dissolution of ions from the NaCl crystals

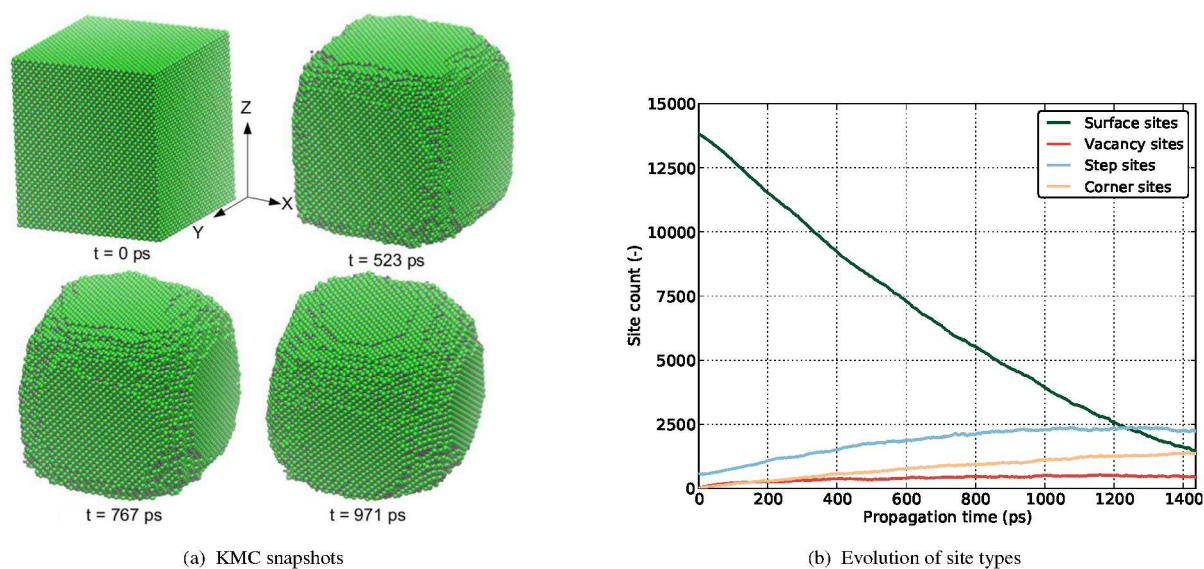


FIG. 6: In (a) the dissolution of the nanocrystal is depicted by using four representative snapshots. The corresponding evolution of the number of surface, vacancy, step and corner (kink) sites is shown in (b).

occurs by ions dissolving from corners or steps and only a very limited fraction from surface or vacancy sites. Nonetheless, in order for an ion to dissolve from a perfect surface, its higher barrier needs to be overcome, which takes a considerable amount of time, and as such limits the dissolution. Consequently, a nanocrystal (with exposed corner and step sites) dissolves much faster.

Even though our approach is rigorous and offers significant insight into the processes involved in dissolution, it has its drawbacks. The computational power required to compute the barriers for each of possible ions and sites is considerable (e.g., one such simulation easily takes about 20 days on 512 processors). In this case we are dealing with a relatively simple system and still we are pushing the computations to the current limits. Applying this method to much larger and complex solid-liquid interface systems seems at the moment to be limited by the computational resources available to us. Alternative approaches based on implicit continuum solvation models may offer a significant improvement in speed, at the cost of losing molecular detail [45–47].

Furthermore, the cost of obtaining the trajectories with the AIMD method makes it difficult to achieve adequate time sampling over the collective water molecules dynamics. This can be best seen in Figure 2(c), where even after averaging over 54 ps, some disparities between equivalent positions with respect to the surface atoms remain. Since the dissolution free energy depends on the re-arrangement of the hydrogen bond network, in order to accommodate and stabilize the dissolved ion, it is expected to be sensitive to inadequate sampling - from comparison of Figure 2(c) with the equivalent density from classical MD run for 50 ns, it is clear that full equilibration has not yet been achieved (or can be in a reasonable time). In order to assess the error introduced, we repeated the constraint calculation with Na^+ ions at three different positions in the $p(4 \times 4)$ NaCl surface, and compare the free energy profiles obtained to the original $p(3 \times 3)$ one in Figure 7. Indeed, the energy profiles vary between surface sites, but in three of the four cases the general shape of the curves is very similar, and the energy barriers are all between 0.5 and 0.6 eV - even for the smaller 3×3 system. One dissolution curve (the red line in Figure 7) leads to a slightly lower energy barrier of 0.4 eV, which still is considerably higher than the closest energy barrier for a different (step) site at 0.26 eV.

Although we used the computed barrier energies in our KMC model, it seems that most of the kinematics follow from the

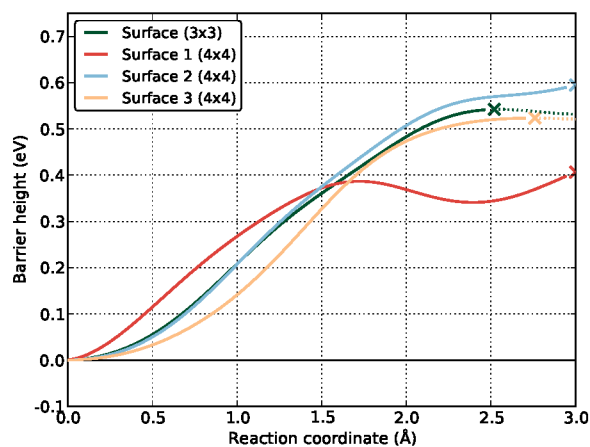


FIG. 7: Different free energy barriers for dissolving an Na^+ ion from a flat surface for four different ions (the green line is the same as in Figure 4(a)). The crosses mark again the maximum value for the respective barrier.

hierarchy in the barrier energies (i.e., surface sites dissolve more unlikely than corner sites), and that the exact numbers play less of role in qualitatively describing the dissolution of an NaCl crystal. This also opens up the possible to use more general KMC models to study dissolution processes of more complex systems, where the AIMD simulations can be used only to assess the hierarchy in energy barriers (without computing the full trajectory) and other parameters might be assessed from classical MD simulations as well. This is of particular interest when recent developments in atomic resolution imaging of surfaces in liquids are considered. The AFM has been a powerful tool for high resolution studies in vacuum for almost two decades [48], especially on NaCl [49, 50], but more recent studies have opened the door to atomic and molecular resolution in liquid environments [51–54]. By rapidly scanning a surface, AFM can also be used to study dissolution processes in real time [55] potentially even in high resolution with the latest techniques. Combining our KMC model with tools for directly simulating high resolution AFM in liquids [56–58] would be a very powerful approach for resolving and proving the details of salt dissolution at the atomic scale.

Acknowledgments

This research has been supported by the Academy of Finland through its Centres of Excellence Program project no. 915804, EU project PAMS (contract no. 610446) and COST Action MP1303. BR has been supported by the Finnish Cultural Foundation (SKR). We acknowledge use of the the Finnish CSC–IT Center for Science’s supercomputing resources. We wish to thank Matthew Watkins for help in setting up the CP2K water simulations.

-
- [1] B. J. Finlayson-Pitts, *Chemical Reviews* **103**, 4801 (2003).
 - [2] S. Piana, M. Reyhani, and J. D. Gale, *Nature* **438**, 70 (2005).
 - [3] S. Piana and J. D. Gale, *Journal Of The American Chemical Society* **127**, 1975 (2005).
 - [4] I. Batyrev, B. Tuttle, D. Fleetwood, R. Schrimpf, L. Tsetseris, and S. Pantelides, *Physical Review Letters* **100**, 105503 (2008).
 - [5] S. Nangia and B. J. Garrison, *Theoretical Chemistry Accounts: Theory, Computation, and Modeling (Theoretica Chimica Acta)* **127**, 271 (2010).

- [6] I. Kurganskaya and A. Lutttge, *The Journal of Physical Chemistry C* **117**, 24894 (2013).
- [7] P. Cabrera-Sanfelix, A. Arnau, G. R. Darling, and D. Sanchez-Portal, *J. Phys. Chem. B* **110**, 24559 (2006).
- [8] P. Cabrera-Sanfelix, A. Arnau, and G. R. Darling, *The Journal of Chemical Physics* **126**, 214707 (2007).
- [9] J. Timko, D. Bucher, and S. Kuyucak, *The Journal of Chemical Physics* **132**, 114510 (2010), URL <http://scitation.aip.org/content/aip/journal/jcp/132/11/10.1063/1.3360310>.
- [10] P. Cabrera-Sanfelix, A. Arnau, G. R. Darling, and D. Sanchez-Portal, *J. Chem. Phys.* **126**, 214707 (2007).
- [11] A. P. Gaiduk, C. Zhang, F. Gygi, and G. Galli, *Chemical Physics Letters* (2014), URL <http://www.sciencedirect.com/science/article/pii/S0009261414003170>.
- [12] E. Stöckelmann and R. Hentschke, *The Journal of Chemical Physics* **110**, 12097 (1999).
- [13] Y. Yang, S. Meng, and E. G. Wang, *J. Phys.: Condens. Matter* **18**, 10165 (2006).
- [14] A. J. Ballard and C. Dellago, *The Journal of Physical Chemistry B* **116**, 13490 (2012).
- [15] K. Kobayashi, Y. Liang, T. Sakka, and T. Matsuoka, *The Journal of Chemical Physics* **140**, 144705 (2014), URL <http://scitation.aip.org/content/aip/journal/jcp/140/14/10.1063/1.4870417>.
- [16] J. L. Aragonés, E. Sanz, and C. Vega, *The Journal of Chemical Physics* **136**, 244508 (2012), URL <http://scitation.aip.org/content/aip/journal/jcp/136/24/10.1063/1.4728163>.
- [17] L.-M. Liu, M. Krack, and A. Michaelides, *J. Am. Chem. Soc.* **130**, 8572 (2008).
- [18] L.-M. Liu, M. Krack, and A. Michaelides, *J. Chem. Phys.* **130**, 234702 (2009).
- [19] L.-M. Liu, A. Laio, and A. Michaelides, *Phys. Chem. Chem. Phys.* **13**, 13162 (2011).
- [20] J. Klimeš, D. R. Bowler, and A. Michaelides, *The Journal of Chemical Physics* **139**, 234702 (2013).
- [21] N. Holmberg, J.-C. Chen, A. S. Foster, and K. Laasonen, *Phys. Chem. Chem. Phys.* **16**, 17437 (2014), URL <http://dx.doi.org/10.1039/C4CP00635F>.
- [22] M. Patra and M. Karttunen, *J. Comput. Chem.* **25**, 678 (2004).
- [23] D. V. D. Spoel, E. Lindahl, B. Hess, G. Groenhof, A. E. Mark, and H. J. C. Berendsen, *J. Comput. Chem.* **26**, 1701 (2005).
- [24] S. Nosé, *J. Chem. Phys.* **81**, 511 (1984).
- [25] W. G. Hoover, *Phys. Rev. A* **31**, 1695 (1985).
- [26] M. Parrinello and A. Rahman, *J. Appl. Phys.* **52**, 7182 (1981).
- [27] H. Shinto, T. Sakakibara, and K. Higashitani, *J. Phys. Chem. B* **102**, 1974 (1998).
- [28] E. Stöckelmann and R. Hentschke, *J. Chem. Phys.* **110**, 12097 (1999).
- [29] A. H. Narten, M. D. Danford, and H. A. Levy, *Discussions Faraday Soc.* **43**, 97 (1967).
- [30] J. VandeVondele, M. Krack, F. Mohamed, M. Parrinello, T. Chassaing, and J. Hutter, *Comput. Phys. Commun.* **167**, 103 (2005).
- [31] J. P. Perdew, K. Burke, and M. Ernzerhof, *Phys. Rev. Lett.* **77**, 3865 (1996).
- [32] J. P. Perdew, J. A. Chevary, S. H. Vosko, K. A. Jackson, M. R. Pederson, D. J. Singh, and C. Fiolhais, *Phys. Rev. B* **46**, 6671 (1992).
- [33] S. Grimme, J. Antony, S. Ehrlich, and H. Krieg, *J. Chem. Phys.* **132**, 154104 (2010).
- [34] S. Woutersen, U. Emmerichs, H.-K. Nienhuys, and H. J. Bakker, *Phys. Rev. Lett.* **81**, 1106 (1998).
- [35] J. D. Eaves, J. J. Loparo, C. J. Fecko, S. T. Roberts, A. Tokmakoff, and P. L. Geissler, *Proceedings of the National Academy of Sciences of the United States of America* **102**, 13019 (2005).
- [36] Y. Yang, S. Meng, and E. G. Wang, *Phys. Rev. B* **74**, 245409 (2006).
- [37] G. Ciccotti, M. Ferrario, J. T. Hynes, and R. Kapral, *Chem. Phys.* **129**, 241 (1989).
- [38] L. Monticelli and E. Salonen, eds., *Biomolecular Simulations: Methods and Protocols* (Springer, 2013).
- [39] J.-L. Li, R. Car, C. Tang, and N. S. Wingreen, *Proc. Natl. Acad. Sci. USA* **104**, 2626 (2007).
- [40] Q. Dai, J. Hu, and M. Salmeron, *J. Phys. Chem. B* **101**, 1994 (1997).
- [41] P. Cabrera-Sanfelix, D. S. Portal, A. Verdager, G. R. Darling, M. Salmeron, and A. Arnau, *J. Phys. Chem. C* **111**, 8000 (2007).
- [42] K. A. Fichthorn and W. H. Weinberg, *J. Chem. Phys.* **95**, 1090 (1991).

- [43] K. A. Fichthorn and M. Scheffler, *Phys. Rev. Lett.* **84**, 53715374 (2000).
- [44] D. A. Bruzewicz, A. Checco, B. M. Ocko, E. R. Lewis, R. L. McGraw, and S. E. Schwartz, *J. Chem. Phys.* **134**, 044702 (2011).
- [45] Y.-H. Fang and Z.-P. Liu, *Journal of the American Chemical Society* **132**, 18214 (2010), <http://pubs.acs.org/doi/pdf/10.1021/ja1069272>,
URL <http://pubs.acs.org/doi/abs/10.1021/ja1069272>.
- [46] Y.-F. Li and Z.-P. Liu, *Journal of the American Chemical Society* **133**, 15743 (2011), <http://pubs.acs.org/doi/pdf/10.1021/ja206153v>,
URL <http://pubs.acs.org/doi/abs/10.1021/ja206153v>.
- [47] K. Mathew, R. Sundararaman, K. Letchworth-Weaver, T. A. Arias, and R. G. Hennig, *Journal Of Chemical Physics* **140**, 084106 (2014).
- [48] F. Giessibl, *Rev. Mod. Phys.* **75**, 949 (2003).
- [49] R. Hoffmann, D. Weiner, A. Schirmeisen, and A. S. Foster, *Phys. Rev. B* **80**, 115426 (2009).
- [50] C. Barth, A. S. Foster, C. R. Henry, and A. L. Shluger, *Adv. Mater.* **23**, 477 (2011).
- [51] T. Fukuma, K. Kobayashi, K. Matsushige, and H. Yamada, *Appl. Phys. Lett.* **87**, 034101 (2005).
- [52] S. Rode, N. Oyabu, K. Kobayashi, H. Yamada, and A. Kuehnle, *Langmuir* **25**, 2850 (2009).
- [53] T. Fukuma, Y. Ueda, S. Yoshioka, and H. Asakawa, *Phys. Rev. Lett.* **104**, 016101 (2010).
- [54] H. Asakawa, S. Yoshioka, K.-i. Nishimura, and T. Fukuma, *ACS nano* **6**, 9013 (2012).
- [55] P. E. Hillner, A. J. Gratz, S. Manne, and P. K. Hansma, *Geology* **20**, 359 (1992).
- [56] M. Watkins and A. L. Shluger, *Phys. Rev. Lett.* **105**, 196101 (2010).
- [57] M. Watkins and B. Reischl, *J. Chem. Phys.* **138**, 154703 (2013).
- [58] B. Reischl, M. Watkins, and A. S. Foster, *J. Chem. Theor. Comput.* **9**, 600 (2013).